

Weighing Superclusters

Chung–Pei Ma

*Department of Physics and Astronomy, University of Pennsylvania,
Philadelphia, PA 19104*

Todd Small

*Institute of Astronomy, University of Cambridge, Madingley Road,
Cambridge CB3 0HA, UK*

Wallace Sargent

*Division of Physics, Mathematics, and Astronomy, California Institute
of Technology, Pasadena, CA 91125*

Abstract. We present a summary report on a detailed study of the mass and dynamical state of the Corona Borealis supercluster using the largest redshift survey of this object to date. Extensive N -body experiments are performed on simulated superclusters in both critically-flat and low-density cosmological models to test the robustness and errors of the mass estimators used on the data. From the redshifts and dynamics of 528 galaxies in the supercluster, the mass of Corona Borealis is estimated to be at least $3 \times 10^{16} h^{-1} M_{\odot}$, and the mass-to-light ratio is $560 h (M/L)_{\odot}$, yielding a matter density parameter of $\Omega_m \approx 0.4$. We also discuss the prospects for mapping the mass distribution on supercluster scales with gravitational lensing.

1. Introduction

Among the most remarkable scientific discoveries of the past decades is the realization that most of the mass in the Universe may reside in dark matter. Although ongoing direct searches for dark matter in particle detectors have not yet revealed positive results, compelling astrophysical evidence for its existence is now abundant. Moreover, various observations now indicate that Nature’s ability to hide dark matter increases with distance scales. A useful measure of this “hiding power” is M/L , the ratio of mass to light of an object expressed in the solar unit $(M/L)_{\odot}$. A larger mass-to-light ratio therefore indicates the presence of more dark matter for the observed amount of light. Current measurements give a mass-to-light ratio of about 5 in the solar neighborhood, 10 in the cores of elliptical galaxies, 100 for the Local group, and as high as 200-300 for clusters of galaxies (e.g., Carlberg et al. 1996). Nature’s appetite appears to be more voracious on grander scales, gobbling up large quantities of matter while exhibiting little sign of digestion.

The motivation for our current study is to obtain measurements of galaxy and matter distributions on the little-explored supercluster scales, and to investigate whether the mass-to-light ratio continues to rise beyond the much-studied cluster scales of a few Mpc. Superclusters are among the largest structures ever registered on maps of the nearby galaxies. Each of these immense clusters of clusters consists of possibly 10,000 or more galaxies in a region of space tens of Mpc across. Our study is focused on the most prominent example of superclustering in the northern sky – the Corona Borealis supercluster, centered at right ascension $15^h 20^m$ and declination $+30^\circ$. This extraordinary cloud of galaxies was already noted by Shane and Wirtanen in 1954 and Abell in 1958. The Corona Borealis supercluster is now known to consist of seven rich Abell clusters at $z \approx 0.07$ and numerous galaxies in the intra-cluster regions. Its core covers a $6^\circ \times 6^\circ$ region of the sky, corresponding to nearly 20×20 Mpc in physical size. Whether the supercluster extends beyond this scale is not yet clear; deeper and wider surveys of the sky will be required to answer this question.

The previous redshift survey of the Corona Borealis supercluster was focused on the densest regions surrounding the cores of six individual Abell clusters A2061, A2065, A2067, A2079, A2089, and A2092 (Postman, Geller, & Huchra 1988). From the dynamics of more than 150 cluster galaxies, the sum of the masses within the central $1 h^{-1}$ Mpc of each of the six clusters was estimated to be $2.4 \times 10^{15} h^{-1} M_\odot$. The mean mass-to-light ratio in the R band for the same region was about 250. If the same M/L is assumed to extend to regions beyond 1 Mpc, the supercluster mass is then $8.2 \times 10^{15} h^{-1} M_\odot$. A higher M/L ratio would further increase the mass.

A more extensive redshift survey of Corona Borealis has since been completed with the 176-fiber Norris Spectrograph at the Palomar 200-inch telescope (Small et al. 1997ab; 1998). This survey substantially increases the number of galaxy redshifts both in the Abell clusters and in the intra-cluster regions. It allows for a more accurate determination of the structure of the supercluster and a more reliable estimate of its mass. A total of 32 fields, each with a 20-arcmin diameter field-of-view, are successfully observed, yielding redshifts for 1491 extragalactic objects. With 163 redshifts from the literature, the entire survey contains 1654 redshifts. A total of 528 galaxies actually lie in the redshift range of the supercluster, $0.06 < z < 0.09$, and forms the sample for the study reported here on the supercluster’s mass and structure. Figure 1 shows the redshift and right-ascension pie diagrams in three declination slices for all galaxies in our survey with $z < 0.15$. The supercluster is well delimited along the line of sight by foreground and background voids. A background supercluster at $z \approx 0.11$ including Abell 2069 is also visible. The foreground galaxies at $z \approx 0.03$ are part of the “Great Wall” identified by Geller and Huchra (1989).

2. Testing Mass Estimators

The main difficulty in estimating the mass of a supercluster is that unlike a star or galaxy cluster, a supercluster is so large that the galaxies and clusters residing in it have not had sufficient time to interact and randomize their motion. It is therefore unclear that traditional estimators such as the virial theorem are valid for a supercluster. In order to address this problem, we have chosen to test the

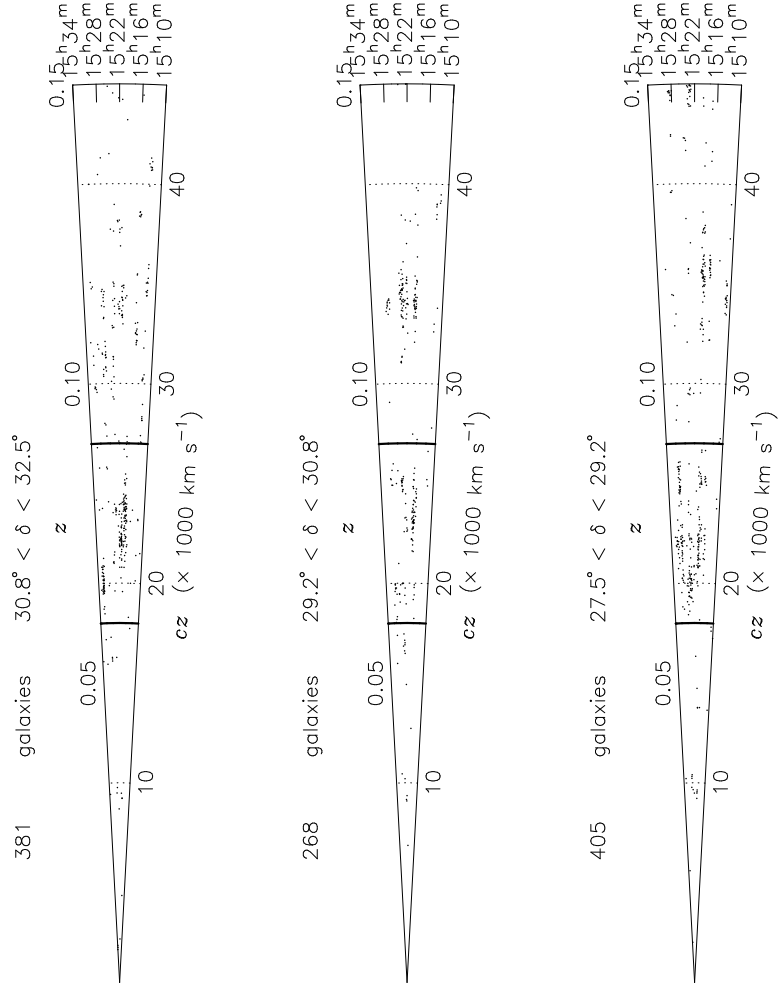


Figure 1. Redshift and right-ascension distribution of all galaxies with redshift $z < 0.15$ in our Corona Borealis survey. The declination range covered by the survey ($27.5^\circ < \delta < 32.5^\circ$) is shown in three slices. The thick lines mark the redshift extent of the Corona Borealis supercluster, while the dotted lines mark the background supercluster.

performance of the virial and other mass estimators on computer-simulated superclusters drawn from large N -body simulations of cosmic structure formation. The simulated superclusters, which are in general quite spatially anisotropic, also enable us to assess the effects of the non-uniform sampling in our observations on our mass estimates.

To anticipate the possibility that supercluster dynamics has a systematic dependence on the cosmological density parameter, we have simulated both critically-flat and low-density models. The $\Omega_m = 1$ model is the standard cold dark matter (CDM) with a Hubble constant of $h = 0.5$ and a normalization of $\sigma_8 = 0.7$ for the rms mass fluctuations in spheres of radius $8h^{-1}$ Mpc. The low-density model is CDM with $\Omega_m = 0.3$, a cosmological constant $\Omega_\Lambda = 0.7$, and $h = 0.75$, normalized to the 4-year COBE quadrupole $Q_{\text{rms-PS}} = 18 \mu K$ (Gorski et al. 1996). The corresponding σ_8 is 1.2. We performed both large-box simulations (640 Mpc a side) with random Gaussian initial conditions and small-box simulations (160 Mpc a side) that are constrained to produce objects with an overdensity of roughly 5. A comoving Plummer force softening length of 160 kpc is used in the particle-particle particle-mesh (P³M) force calculation for all simulations.

Figure 2 shows the dark matter distribution in one simulated supercluster. Each side of the box shown is 30 Mpc, and the total mass is $1.1 \times 10^{16} M_\odot$. This object is extracted from a large cosmological simulation of the CDM model that traced the motion of 17 million particles in a $(640 \text{ Mpc})^3$ box. The average overdensity in this region is $\delta\rho/\rho = 4.7$. We identified 15 other supercluster-like objects that emerged in our cosmological simulations of both $\Omega_m = 1$ and $\Omega_m = 0.3$ models. To minimize a potential selection bias, only two criteria are applied in identifying these objects. First, the candidates must consist of multiple dark matter halos that have not yet merged into one dominant smooth halo. This feature is strongly suggested by the observed complex substructure (e.g., the Abell clusters) of the Corona Borealis. The only other criterion is that the objects have an average overdensity of ~ 5 in a volume of $\sim 30^3 \text{ Mpc}^3$, corresponding to the least evolved dynamical state of Corona Borealis (see below). This is a conservative choice since systems with higher overdensities are closer to virialization, and the mass estimators should only work better.

For the virial estimator, the mass is calculated from

$$M_V = \frac{3\pi}{G} \sigma^2 \left\langle \frac{1}{r_p} \right\rangle^{-1}, \quad (1)$$

where σ is the line-of-sight velocity dispersion and $\langle 1/r_p \rangle^{-1}$ is the mean harmonic projected separation. A simple estimator for $\langle 1/r_p \rangle^{-1}$ is given by

$$\left\langle \frac{1}{r_p} \right\rangle^{-1} = \frac{D}{2} N(N-1) \left(\sum_i \sum_{j < i} \frac{1}{\theta_{ij}} \right)^{-1}, \quad (2)$$

where θ_{ij} is the angular separation of galaxies i and j , D is the radial distance, and N is the total number of galaxies. This estimator, however, is very sensitive to close pairs and is thus quite noisy, especially for systems which have not been

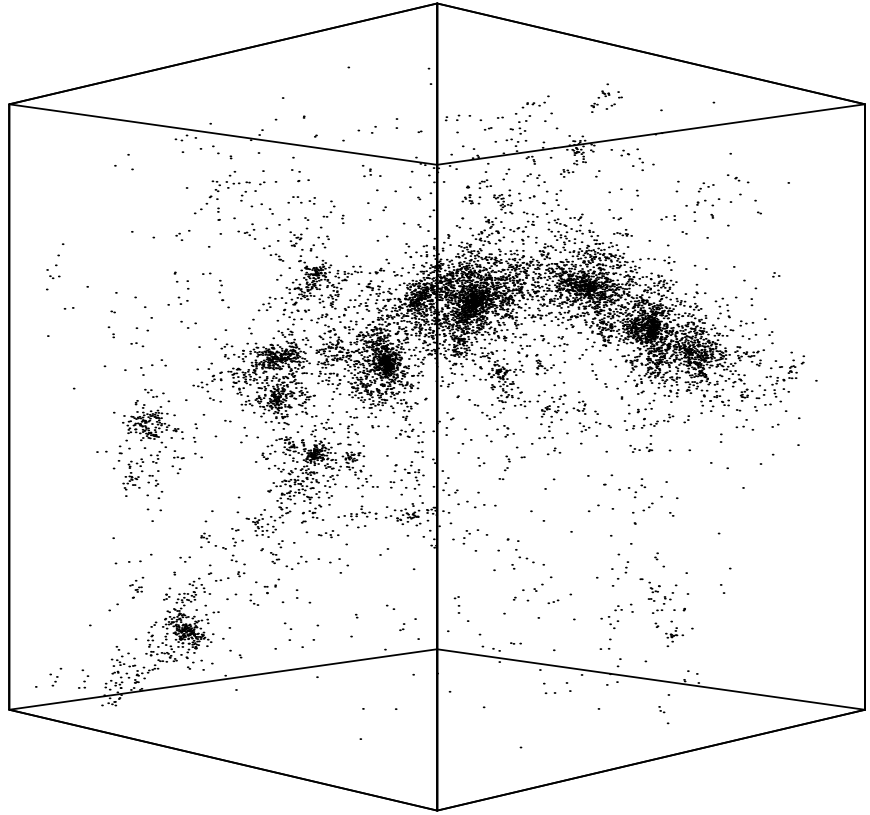


Figure 2. An example of the simulated superclusters used to test the mass estimators applied on the actual data. This complex structure consists of at least 7 cluster-type subclumps, each with a mass exceeding $2 \times 10^{14} M_{\odot}$. Each side of the cubic box is 30 Mpc, and the total mass inside the box is $1.1 \times 10^{16} M_{\odot}$.

uniformly sampled spatially. We adopt an alternative estimator introduced by Carlberg et al. (1996) that is less sensitive to irregular sampling and close pairs:

$$\left\langle \frac{1}{r_p} \right\rangle = \frac{N(N-1)}{2} \sum_i \sum_{j<i} \frac{2}{\pi(r_i+r_j)} K(k_{ij}), \quad (3)$$

where r_i and r_j are the projected radii of objects i and j , $K(k)$ is the complete elliptic integral of the first kind in Legendre’s notation, and $k_{ij}^2 = 4r_i r_j / (r_i + r_j)^2$. Although this “ringwise” estimator was originally developed for systems such as galaxy clusters with near circular symmetry on the sky, we find this estimator to give less biased values of $\langle 1/r_p \rangle^{-1}$ than the straightforward sum in equation (2).

We have also tested the projected mass estimator (Bahcall & Tremaine 1981) given by

$$M_P = \frac{f_{\text{pm}}}{GN} \sum_i v_i^2 r_i. \quad (4)$$

It is designed to give equal weights to particles at all distances (if $v^2 \propto 1/r$ on the average), but the estimate depends on the mean eccentricity of the particle orbits parameterized by f_{pm} . It can be shown that $f_{\text{pm}} = 32/\pi$ for isotropic orbits and $64/\pi$ for radial orbits, independent of the mass distribution (Heisler, Tremaine, & Bahcall 1985). We have chosen to use $f_{\text{pm}} = 32/\pi$ since this yields the smallest masses.

Table 1 summarizes our test statistics on the 16 simulated superclusters in both $\Omega_m = 1$ and 0.3 models. Each supercluster is projected onto a two-dimensional sky, and the masses are computed from eqs. (1) and (4) using all the particles in the supercluster. Overall, we find that the virial theorem works remarkably well at recovering the true mass M_T of the simulated superclusters. An important result is that the estimators do not perform worse in the $\Omega_m = 0.3$ model as one may have expected for a low-density model.

To test the effects of irregular sampling in our redshift survey, we have also conducted simulated observations of these model superclusters with strategies similar to those used during the actual observations. Each supercluster is projected onto a two-dimensional sky and portions of it are viewed through randomly-placed fictitious observing fields. Instead of using all particles, a fraction of them in each field are randomly rejected so that the total number of particles used in the simulated observations was roughly 500, comparable to the number of galaxies with measured redshifts in Corona Borealis. We find the non-uniform sampling to systematically underestimate $\langle 1/r_p \rangle^{-1}$ but does not significantly affect the velocity dispersion. Overall, the virial estimator underestimates the true mass by 31% in the $\Omega_m = 1$ model and by 5% in the $\Omega_m = 0.3$ model. Based on this result and Table 1, we conclude that the virial and projected mass estimators can be reliably applied to superclusters even though they are not relaxed systems. With our irregular sampling, the estimators may underestimate the true mass by up to 30%.

An interesting question to ask is why the virial (or similar) mass estimator works so well for unrelaxed objects with prominent substructure such as in Figure 2. An important clue is that our 16 simulated superclusters all turned out to be gravitationally bound even though this was *not* a selection criterion.

Table 1. Test results of mass estimators

Model	$\langle M_V/M_T \rangle^a$	$\langle M_P/M_T \rangle^b$
$\Omega_m = 1$	0.94 ± 0.24	0.76 ± 0.24
$\Omega_m = 0.3$	0.99 ± 0.21	1.04 ± 0.52

^aRatio of virial mass M_V of eq. (1) to true mass.

^bRatio of projected mass M_P of eq. (4) to true mass.

How well does the virial estimator work for a bound system? For a random collection of particles, the virial theorem clearly can yield a mass that is wrong by an arbitrary factor. For a bound system with $K - |W| < 0$ (where K and W are the kinetic and potential energy), however, it is easy to show that the virial mass M_V can never exceed twice the system's true mass M_T . (Recall a virialized system has $K = |W|/2$.) In fact, M_V approaches $2M_T$ only for a marginally bound system with $K \approx |W|$. For systems with $|W|/2 < K < |W|$, one gets $M_T < M_V < 2M_T$; while for systems with $K < |W|/2$, the virial estimator underestimates the mass: $M_V < M_T$. The virial theorem can therefore recover the true mass of a *bound* system to within a factor of 2 in most cases. We indeed find this statement to be true for all 16 simulated superclusters.

Although our N -body experiments strongly suggest that superclusters are generally bound objects, we provide an additional argument here supporting the possibility that the Corona Borealis supercluster is gravitationally bound. The spherical tophat model for gravitational collapse indicates that an outer shell of a density perturbation is bound if the mean overdensity within the shell is greater than $(\Omega_m^{-1} - 1)/(1 + z)$ (e.g., Peebles 1980). Taking 0.3 to be a rough lower limit on Ω_m , a supercluster at $z = 0.07$ must be overdense by more than a factor of 2.1 for it to be bound. In comparison, the observed overdensity in galaxy counts in Corona Borealis relative to the field is $\delta \approx 7f$, where the dimensionless parameter f , defined by $f \equiv c \delta z / H_0 \delta r$, measures the relative elongation in redshift space δz and real space δr along the line of sight. The minimal value of f is unity, corresponding to zero peculiar velocities, whereas a larger f indicates a stronger “finger-of-god” effect due to galaxy peculiar motion. Although we cannot completely rule out the $f = 1$ case, it is very difficult to arrange an object that is as immense and prominent as the Corona Borealis while at the same time is freely expanding with the Hubble flow without exhibiting any peculiar velocities. The overdensity in galaxy counts in the Corona Borealis is therefore at least 7, but more likely to be significantly above this value. The Corona Borealis supercluster is therefore bound unless galaxies are significantly biased relative to mass by more than a factor of 3.5.

3. Mass and M/L of Corona Borealis

Given the robustness of the mass estimators found in our numerical tests described in the previous section, we now proceed to apply eqs. (1)-(4) to the actual

data from the Corona Borealis survey. Using the techniques of Beers, Flynn, & Gebhardt (1990), we estimate the centroid velocity of the Corona Borealis supercluster to be $c\bar{z} = 22420_{-138}^{+149}$ km s⁻¹ and the dispersion to be $\sigma = 1929_{-67}^{+81}$ km s⁻¹ in the cluster rest frame. Using the ringwise estimator in eq. (3), we find $\langle 1/r_p \rangle^{-1} = 4.6 h^{-1}$ Mpc. The virial mass estimator (eq. (1)) then gives a mass of $3.8 \times 10^{16} h^{-1} M_\odot$ for the Corona Borealis supercluster. The projected mass estimator in eq. (4) yields a similar value, $4.2 \times 10^{16} h^{-1} M_\odot$. Based on the tests described in the previous section, we conclude that a secure lower bound to the mass of the Corona Borealis supercluster is $3 \times 10^{16} h^{-1} M_\odot$.

The supercluster luminosity function for $M(B_{AB}) \leq -16.3 + 5 \log h$ mag in the AB-normalized B band is presented in Small et al. (1997b). Integration of the luminosity function yields a mean luminosity density of $\rho_L(B_{AB}) = 1.9 \times 10^9 h L_\odot \text{ Mpc}^{-3}$ in the supercluster. Taking the solid angle of the survey to be 0.0076 sr (= 25 deg²) and the redshift limits of the supercluster to be at $z = 0.06$ and 0.09, the volume of the region surveyed is $2.8 \times 10^4 h^{-3} \text{ Mpc}^3$. The M/L ratio of the supercluster in the B_{AB} band is thus $560 h (M/L)_\odot$. For a local B_{AB} -band luminosity density of $(1.8 \pm 0.2) \times 10^8 h L_\odot \text{ Mpc}^{-3}$ for $M(B_{AB}) < -16 + 5 \log h$ mag (Small et al. 1998 and references therein), the corresponding critical M/L ratio to close the universe is $1550 \pm 170 h (M/L)_\odot$. We therefore obtain $\Omega_m = 0.36$ for the density parameter on supercluster scales of $\sim 20 h^{-1}$ Mpc.

4. Future Prospects

Our determination of M/L and Ω_m on supercluster scales can be strengthened by measurements of other superclusters with techniques similar to those described above, or by independent measurements with alternative mass-estimating methods. The former will be achieved when the ongoing large-area redshift surveys (such as the 2dF and Sloan surveys) generate sufficient data. For the latter, a very powerful technique is gravitational lensing, which probes the mass profile of a foreground object by the gravitational distortion it induces on the images of background objects. A galaxy cluster, for example, induces a correlated elliptical distortion in the images of background galaxies. Measurements of such statistical signals over many galaxies have been used successfully to map the surface mass densities of individual clusters (e.g., Tyson et al. 1990; Kaiser & Squires 1993; Mellier et al. 1996 and references therein). Extending the gravitational lensing technique to superclusters will be a promising alternative probe of the dark mass distribution on such large length scales.

Figure 3 is an illustration of the lensing signal expected in a superclustering region. The left panel shows the particle distribution in a different projection of the same simulated supercluster in Figure 2. Each bar in the right panel shows the local strength and direction of the theoretical elliptical distortion in the shapes of the background galaxies due to lensing by the supercluster. More explicitly, if the two-dimensional gravitational potential is denoted by ψ , and $\gamma_1 \equiv (\partial_x^2 - \partial_y^2)\psi/2$ and $\gamma_2 \equiv \partial_x \partial_y \psi$, then the magnitude of each bar is proportional to the shear $\gamma \equiv (\gamma_1^2 + \gamma_2^2)^{1/2}$ that measures the anisotropic stretching of the images. The angle β of each bar relative to the horizontal axis obeys

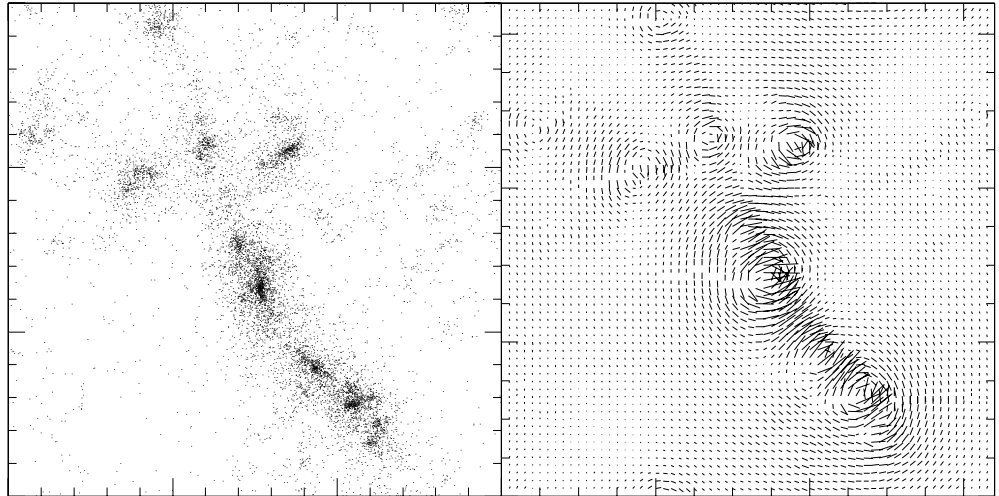


Figure 3. Left: A different projection of the simulated supercluster shown in Figure 2. Each side of the box is 30 Mpc, and the total mass in the box is $1.1 \times 10^{16} M_{\odot}$. Right: The local magnitude and orientation of the shear field induced by the supercluster.

$\tan(2\beta) = \gamma_2/\gamma_1$. Comparison of the two figures shows that the amplitude of the distortion on the right is clearly correlated with the projected mass density on the left, and the preferential tangential alignment of the shear orientation is evident. A promising feature is that the shear amplitudes do not drop appreciably along the ridges connecting individual cluster-like clumps. Measurements of the distortion in the images of background galaxies can therefore in principle be used to construct a surface mass density map in a supercluster. This offers a powerful alternative way to probe the distribution of dark matter on scales of tens of Mpc.

Acknowledgments. We are grateful to the Kenneth T. and Eileen L. Norris Foundation for their generous grant and Donald Hamilton for construction of the Norris Spectrograph. We thank Jim Frederic and Paul Bode for aid with the N -body simulations, and Roger Blandford and David Buote for helpful comments. Supercomputing time was provided by the National Scalable Cluster Project at the University of Pennsylvania, the National Center for Supercomputing Applications, and the Cornell National Supercomputer Facility. This work has been supported by an NSF Graduate Fellowship (TAS), a Caltech PMA Division Fellowship (CPM), and NSF grant AST92-213165 (WLWS).

References

- Abell, G. 1958, *ApJS*, 3, 211
Bahcall, J., & Tremaine, S. 1981, *ApJ*, 244, 805
Beers, T., Flynn, K., & Gebhardt, K. 1990, *AJ*, 100, 32

- Carlberg, R., Yee, H., Ellingson, E., Abraham, R., Gravel, P., Morris, S., & Pritchett, C. 1996, *ApJ*, 462, 32
- Geller M., & Huchra, J. 1989, *Science*, 246, 897
- Gorski K. et al. 1996, *ApJ*, 464, L11
- Heisler, J., Tremaine, S., & Bahcall, J. 1985, *ApJ*, 298, 8
- Kaiser, N. & Squires, G. 1993, *ApJ*, 404, 441
- Mellier, Y., van Waerbeke, L., Bernardeau, F., & Fort, B. 1996, astro-ph 9609197
- Peebles, P. 1980, *The Large-scale Structure of the Universe*, Princeton: Princeton University Press
- Postman, M., Geller, M., & Huchra, J. 1988, *AJ*, 95, 267
- Shane, C. & Wirtanen, C. 1954, *AJ*, 59, 285
- Small, T., Sargent, W., & Hamilton, D. 1997a, *ApJS*, 111, 1
- Small, T., Sargent, W., & Hamilton, D. 1997b, *ApJ*, 487, 512
- Small, T., Ma, C.-P., Sargent, W., & Hamilton, D. 1998, *ApJ*, 492, 45
- Tyson, J., Valdes, F., & Wenk, R. 1990, *ApJ*, 349, L19